

Recovering CMB polarization maps with neural networks: Performance in realistic simulations

J. M. Casas,^{a,b,1} L. Bonavera,^{a,b} J. González-Nuevo,^{a,b} G. Puglisi,^{c,d} C. Baccigalupi,^{e,f} S. R. Cabo,^{a,b} M. M. Cueli,^{e,f} D. Crespo,^{a,b} C. González-Gutiérrez,^{g,b} F.J. de Cos^{h,b}

^aDepartamento de Física, Universidad de Oviedo,
C. Federico García Lorca 18, 33007 Oviedo, Spain

^bInstituto Universitario de Ciencias y Tecnologías Espaciales de Asturias (ICTEA),
C. Independencia 13, 33004 Oviedo, Spain

^cDipartimento di Fisica e Astronomia, Università degli Studi di Catania,
Via S. Sofia, 64, 95123, Catania, Italy

^dINFN – Sezione di Catania,
Via S. Sofia 64, 95123 Catania, Italy

^eSISSA,
Via Bonomea 265, 34136 Trieste, Italy

^fINFN-Sezione di Trieste,
Via Valerio 2, 34127 Trieste, Italy

^gDepartamento de Informática, Universidad de Oviedo,
Edificio Departamental 1. Campus de Viesques s/n, E-33204, Gijón, Spain

^hEscuela de Ingeniería de Minas, Energía y Materiales, Universidad de Oviedo,
C. Independencia 13, 33004 Oviedo, Spain

E-mail: casasjm@uniovi.es

Abstract. Recovering the polarized cosmic microwave background (CMB) is crucial for shading light on the exponential growth of the very early Universe called Cosmic Inflation. For achieving this task, not only improving the instrument sensitivities but also mathematical methods with different natures should be developed. In this work we aim to use a neural network previously and accurately tested with Planck realistic temperature simulations called the CMB extraction neural network (CENN), and train it for recovering both Q and U maps. After mixing them into E and B modes, we found a mean absolute error of about $0.1 \pm 0.3 \mu K^2$ for both, and residuals of $10^{-1} \mu K^2$ up to $l \sim 1000$, after smoothing the maps with a $15'$ FWHM. In an ideal case (without instrumental noise) we recover the signal with a similar error but lower residuals in the output maps. We also found that residuals decrease when smoothing the maps with larger FWHM, although we lose the smaller scales. Based on these results, we conclude that neural networks could be worth using as component separation methods for polarization data, especially for future CMB experiments with higher sensitivity than Planck.

¹Corresponding author.

Contents

1	Introduction	1
2	Simulations	2
3	Methodology	2
4	Results	4
4.1	Ideal case	4
4.2	Realistic case	5
4.3	Additional tests	7
5	Conclusions	8

1 Introduction

The cosmic microwave background (CMB) has been help these last decades the scientific community to understand the nature and evolution of the Universe. It is an emission produced at about 380000 years after the Big Bang, when photons decoupled from baryons, an epoch called recombination [1]. Isotropic at first order, it has indeed small deviation in temperature and polarization called anisotropies. They can be described by approximating the celestial sphere with the Stokes Q and U parameters [2], and in particular its polarization by mixing both parameters into gradient and curl modes, known as E and B modes respectively [3]. Thus, the E modes are associated with scalar (density) perturbations in the early universe, while the B modes are sourced by tensor (gravitational) perturbations, which arise from the gravitational lensing of the CMB by intervening large-scale structure, as so as inflationary gravitational waves.

In these last decades, different experiments have reconstructed the CMB maps with high accuracy. In particular, the Planck mission [4] has observed the microwave sky during the last decade and published unprecedented detailed maps, which help to constrain the main properties of the Universe, as so as the main microwave emissions from our Galaxy, especially in temperature maps. Future experiments like the Simons Observatory [5] and LiteBIRD [6], an many more, are planned to constrain the main properties of the CMB polarization, and in particular the B mode power spectrum at large scales, as so as the search for primordial gravitational waves in the cosmological spectra.

Once experiments with higher sensitivity than Planck start their observations, the main problem will be to properly have characterize the microwave sky, since the CMB polarization is contaminated at all sky regions and scales by Galactic and extra galactic emissions, especially if the target is to constrain the tensor-to-scalar ratio between B and E modes to $r = 0.001$ ([7], [8]). A precise knowledge of the polarization properties of these emissions called foregrounds will allow methods to properly separate the CMB signal with respect the other ones. Such process is called component separation. Although several different models are now tested and improved to be ready for the challenges of the next decade (the main ones are described in detail in [9]), machine learning models like neural networks have still been initially tested against this kind of data, although they have demonstrated promising results

in other astronomical fields [10]. These networks therefore seem promising for these type of analyses due to their ability to learn non-linear behaviors from data [11] and thus discern between the different complex physical behaviors of the emissions forming the microwave sky.

Before this work, a few ones have shown that neural networks could be a promising tool for recovering the CMB signal in microwave simulations, in both temperature ([12], [13]) and polarization [14] maps. Another promising methodology was firstly presented in [15] and been applied on realistic temperature simulations of the Planck experiment, which is in fact an analysis extended to polarization realistic simulations in this work. Thus, it is organized as follows: Section 2 describes the simulations we use for training and validating the network, Section 3 summarizes the adopted methodology, Section 4 shows our results, and finally Section 5 describes our conclusions.

2 Simulations

For training and validating the network we use realistic simulations of the microwave sky as seen by the HFI Planck instrument at 100, 143 and 217 GHz, since they were the channels less contaminated by noise (1.96, 1.17 and 1.75 μK deg for each channel, respectively [4]).

We consider for the simulations a lensed CMB map plus Galactic interstellar dust and synchrotron emission. These three set of maps were downloaded from the Planck Legacy Archive website (PLA¹), which are based on foreground models updated from the third release of Planck data [16]. Since we use along this work a convolutional neural network, we have to work with sky patches for training and validation. Therefore, the maps are cut into quadratic patches of 256×256 pixels, with a pixel size of 90 arcseconds, by using the methodology described in [17]. We thus inject, for completeness, extragalactic radio sources to these patches by using [18] model and the software CORRISKY [19]. Finally, we add white instrumental noise at Planck levels.

We then construct for each position three patches called Input Total formed by all the emissions plus noise at 100, 143, 217 GHz, and we also save the CMB patch, that we call the label, at 143 GHz. The training set is formed by a total of 10000 simulations, and each validation set has 1000 simulations not used for training. An example of the simulated patches is shown in Figure 1.

3 Methodology

An artificial neural network is a kind of machine learning model formed by computational units called neurons that are organized in layers. Neurons are formed by weights which vary their value while the network is trained. At the end of the architecture, after the train data flows along all the layers, a loss function is minimized to give an optimal gradient value that updates all the weights of the network layers. Then, it starts a new training epoch. This is then an optimization problem.

Neural networks also performs on image data (which are indeed 2-dimensional matrices), for example on image segmentation problems [20]. In this case, weights are also matrices and they are called Kernels. In this work we extend the cosmic microwave background extraction neural network (CENN) firstly presented in [15] to evaluate their performance on polarization realistic simulations.

¹<http://pla.esac.esa.int/pla/#home>

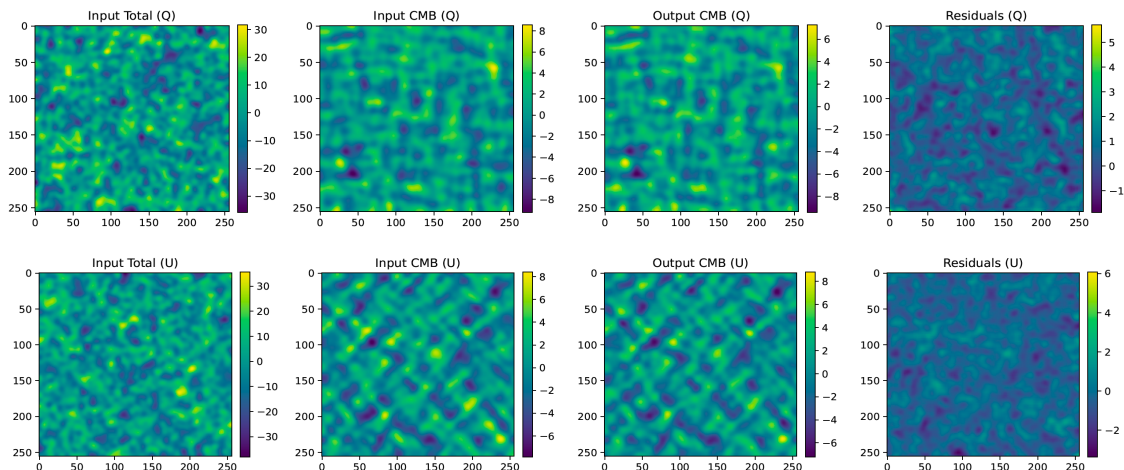


Figure 1. Example of one realistic simulation used in this work. From left to right: Input Total patch formed by all the simulated emissions, the input CMB, which is also part of the Input Total patch, the output CMB from the network and the residual patch, formed by the difference between input and output ones. The units in all the colorbars are μK .

CENN is a fully-convolutional neural network based on the U-Net architecture [21] with the ability of produce clean CMB maps from noisy sky patches. The details of how these kind of neural networks are able to perform image segmentation on multi-frequency data are explained mathematically and physically in [22] and [15] respectively, and the reader is encouraged to look for these works. However, it is also useful to have here a brief description of the network architecture and behavior.

Firstly, the network reads the Input Total patches. Their information is mixed and convolved in six consecutive blocks with the network's filters along several feature maps. An activation function allows some of the non-linear information to pass through. After the last block, the information is then deconvolved with more filters in 6 more consecutive blocks, which are also connected to each convolutional one, discerning which structures along the inferred patch are similar or different to the input ones. In the final block, the information is finally mixed into one patch formed by the output CMB. These values are used to minimize a loss function. This computes a gradient, which updates the filter and the weight values of all the architecture using the backpropagation algorithm. Then it starts a new epoch of training.

The exact architecture is shown in Figure 2 and it is detailed as follows: firstly, it has a set of six convolutional blocks, all of them formed by convolutional and pooling layers with 8, 2, 4, 2, 2, and 2 kernels of sizes of 9, 9, 7, 7, 5, and 3, respectively. The number of filters is 8, 16, 64, 128, 256, and 512, respectively. They have a subsampling factor of 2. The padding type "Same" is added in all the layers in order to add some space around the input data or the feature map, to deal with possible loss in width and/or height dimension in the feature maps after having applied the filters. The activation function is leaky ReLU in all the layers. Secondly, the network has a set of six deconvolutional blocks that are formed by deconvolutional and pooling layers with 2, 2, 2, 4, 2, and 8 kernels of sizes of 3, 5, 7, 7, 9, and 9, respectively. The number of filters is 256, 128, 64, 16, 8, and 1. Their subsampling factor is 2. The padding type "Same" is also added in all the layers, and the activation function is, as for the convolutional blocks, the leaky ReLU one.

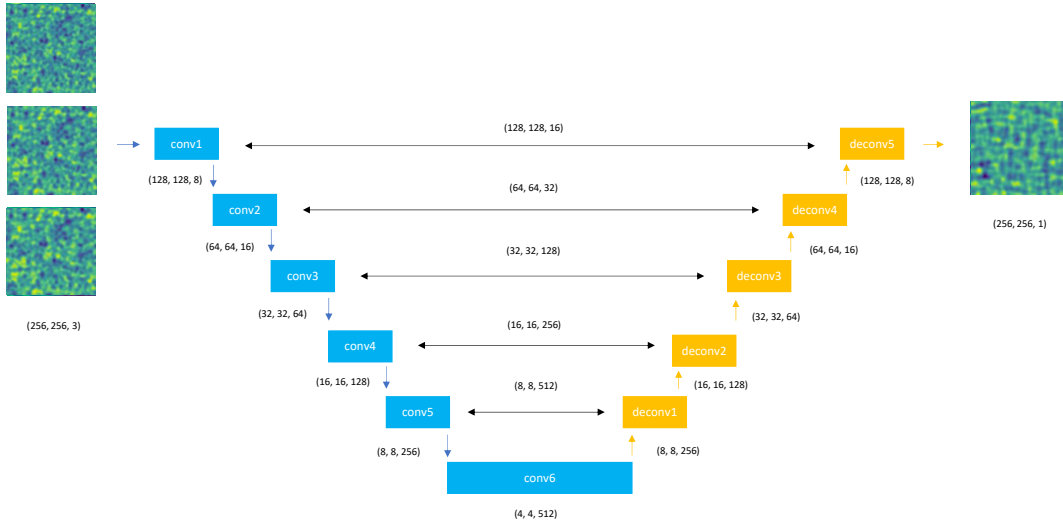


Figure 2. Architecture of CENN, the neural network used in this work. We show for visualization purposes the kind of input and output patches the network reads and outputs, respectively.

4 Results

This section presents our results after validating the network with simulations of the sky as seen by Planck. We have decided to analyze the performance of the network in a similar way as in the previous work with total intensity simulations [15], which is by comparing the input CMB, i.e. the CMB spectra in the validation simulations, with the output CMB from the neural network and the residual power spectra, estimated as the spectra of the difference between input and output, which is representative of the structures not recovered by the network.

Subsection 4.1 summarizes the performance of the network in an ideal case, i.e. the CMB is contaminated by foregrounds but without adding instrumental noise. Subsection 4.2 shows a similar analysis but for a realistic case, i.e. adding instrumental noise to the CMB plus foreground maps, and Subsection 4.3 covers some additional tests for completeness.

4.1 Ideal case

Firstly, we train and validate the network in an ideal case, with simulations only containing CMB and foregrounds, and without foregrounds. Thus, after validating the network, we obtain 1000 Q and U patches, and then we mix them both and estimate the average E and B spectra of the residual maps with NaMaster [23], which are represented in Figure 3 (in black at both left and right panel, respectively) compared against the input and output CMB (in blue and red, respectively). Shaded areas represent the 1σ standard deviation for each bin.

As shown, on the one hand, we found a mean absolute error (in brown at the bottom subpanels) of about $0.1 \pm 0.3 \mu K^2$ for both modes. On the other hand, residuals are generally below the input signal. In particular their mean is between 10^{-2} and $10^{-1} \mu K^2$ for E and around $10^{-2} \mu K^2$ for B , which means that residual values are around two orders of magnitude

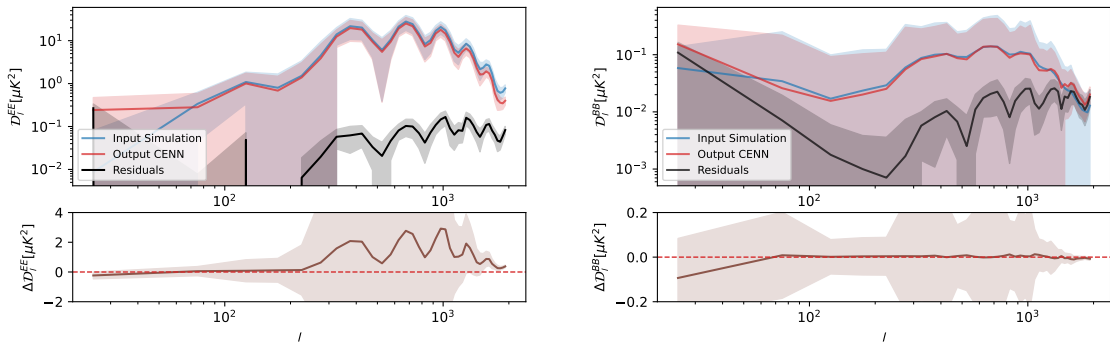


Figure 3. E and B mode power spectra recovering with CENN in an ideal case. Top left panel: comparison between the input E mode (in blue) and the output from the network (in red). The residuals are shown in black. The bottom left panel represents the absolute difference between input and output spectra. Right panel describes the same analysis but for the B mode. Shaded areas show the 1σ standard deviation for each bin.

below the input E signal and one order below B . Despite representing the remaining structures after the network’s processing, these residuals, which are substantially lower than the input signal, suggest that the network effectively suppresses a significant portion of the foreground contamination, although some level of unseparated components, notably interstellar dust (given the analyzed frequencies) is still present in the output, especially at the largest scales.

While the limited patch size of approximately 6.4 square degrees impacts the statistical significance of our results at the largest scales, it is important to note that these findings remain relevant for understanding the network’s performance. As said before, our analysis reveals a clear excess in the power spectra for $l < 80$, which we attribute to residual foreground contamination, likely from interstellar dust, given the frequencies analyzed. We anticipate that the performance of CENN at these large scales could be improved by employing larger patch sizes. However, our investigations into this approach have uncovered a strong E -to- B leakage when projecting larger patches onto the plane, a technical challenge that need further investigation and correction before the benefits of larger sky areas can be fully realized.

The findings presented here demonstrate that a relatively straightforward fully convolutional neural network architecture like CENN exhibits competitive capabilities in performing a kind of component separation process on simulated polarized CMB maps. This suggests that even with a non-elaborate network structure, machine learning techniques can offer a promising avenue for effective foreground mitigation in CMB polarization data, warranting further investigation for their potential in future high-sensitivity experiments.

4.2 Realistic case

Considering the promising results summarized in the previous section, we decided to analyze the performance of the network in a more realistic situation by following a similar approach but adding white instrumental noise into the patches at Planck levels (1.96, 1.17 and 1.75 $\mu K \text{ deg}$ for 100, 145 and 217 GHz, respectively [4]). We thus re-train the neural network with those more realistic Planck-like simulations. Before training, we smooth the data with a 15’ FWHM to increase the signal-to-noise ratio, which is indeed a common practice in CMB

recovery and component separation analyses ([24], [25] and references therein). This will allow us to analyze the spectra up to multipoles $l \sim 1000$.

Figure 4 presents the network performance, being the used colors representing the same metrics. In this case, we found for both E and B modes a mean absolute error of about $0.1 \pm 0.3 \mu K^2$, and residuals of $10^{-1} \mu K^2$, which means similar uncertainties than in the previous case but with higher residuals, although the simulated foreground contamination remained consistent with the ideal case. This seems to be principally related to the noise injection, which 143 GHz spectra² is represented as a green dotted line: the residuals seem to be structures in the output patch that mimic the CMB ones after the smoothing step but they could not be properly separated by the network. This finding carries significant implications for future CMB experiments boasting higher sensitivity, as it suggests that with reduced instrumental noise, the performance of CENN in recovering the CMB polarization could potentially approach the lower residual levels observed in the ideal, noise-free simulations. This indicates a promising outlook for the application of neural networks like CENN in next-generation CMB surveys.

Furthermore, the fact that residual levels at large scales remained comparable to the ideal case suggests that the presence of instrumental noise does not significantly hinder CENN’s ability to mitigate foregrounds at these angular scales. As previously discussed in Section 4.1, the limitations at large scales appear to be more intrinsically linked to the finite patch size and the inherent challenges in separating foreground components like interstellar dust, which are not substantially exacerbated by the addition of Planck-level instrumental noise.

Moreover, as observed in Figure 4, the B mode remains more susceptible to both instrumental noise and foreground contamination, a fact highlighted by the comparison of residuals with respect to the network’s output. However, the orange line, representing the difference between the CENN output and the residuals, effectively traces the estimated recovered CMB signal. Its proximity to the output spectrum suggests that CENN, even when the CMB signal is subdominant to instrumental noise, demonstrates a tendency to preserve the recovered CMB signal. This behavior indicates a robustness in the methodology, where the network appears to prioritize minimizing alterations to the underlying CMB signal, potentially at the expense of a more aggressive removal of the dominant noise. Consequently, this implies that the level of the recovered CMB signal in the output can be considered a reliable estimate, likely representing an upper bound on the true CMB signal even in the presence of significant instrumental noise.

Given that CENN demonstrates a tendency to preserve the underlying CMB signal within its output, it would theoretically seem plausible to further refine these outputs by attempting to isolate the CMB component from the remaining residuals. To explore this possibility, we tested the approach of using a secondary neural network, where the input consisted of the CENN output maps and the label was the original CMB signal, with the aim of training it to remove the residual structures. However, the fact that we obtained similar results to the initial CENN output suggests that we are likely encountering the statistical limitations inherent in the Planck-like data, particularly concerning the low signal-to-noise ratio for the B modes. Therefore, with the current CENN architecture and the noise levels present here, it appears that we are approaching the limit of what can be reliably extracted, and further improvements in component separation for these specific data conditions may

²We decided to show only in the Figures along the manuscript the noise contribution at 143 GHz, i.e. at the same frequency we trained the network to output the CMB, not only for visualization purposes but also because we are directly comparing with the estimates for that frequency.

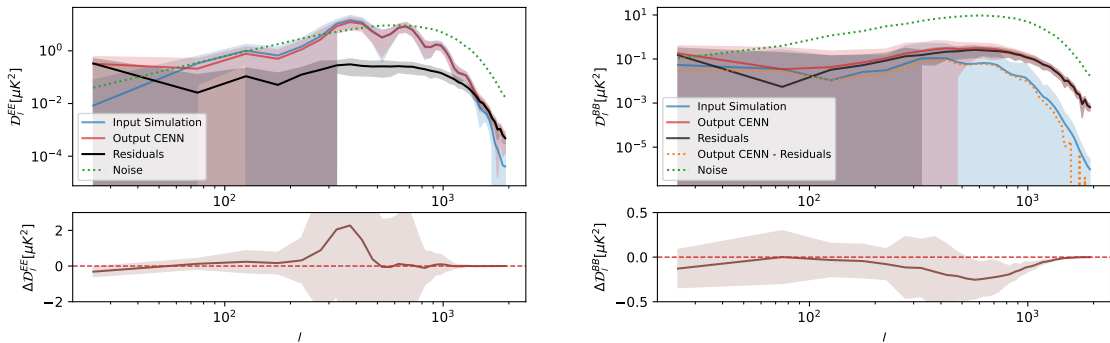


Figure 4. E and B mode power spectra recovering with CENN in a realistic case at $15'$ FWHM. Top left panel: comparison between the input E mode CMB spectra (in blue) and the output from the network (in red) The residuals are shown in black. Green dotted line represents the noise levels at 143 GHz. The bottom left panel represents the absolute difference between input and output spectra. Right panel describes the same analysis but for the B mode. The difference between output and residual spectra is plotted in the orange dotted line. Shaded areas show the 1σ standard deviation for each bin.

necessitate more sophisticated methodologies or data with intrinsically higher signal-to-noise ratios.

As a first-approximation comparison with the traditional component separation methods used in Planck (SMICA, NILC, Commander, and SEVEM³), we obtain similar results than them for the E mode, since they estimated the spectra with a mean absolute error between 0 and $1 \mu K^2$, and a standard deviation between 5 and $6 \mu K^2$ in similar realistic simulations, but smoothed at $10'$ FWHM [26], as so as the spectra was accurately recovered up to $l \sim 700$, where noise started to dominate the signal. For the B mode, traditional methods could not estimate the signal nor give an upper limit and we cannot directly compare with them, at least for this kind of data.

4.3 Additional tests

To further assess the robustness of the CENN methodology and explore potential avenues for result enhancement, we conducted additional tests beyond the primary analysis presented in the preceding sections. Given the established utility of smoothing in CMB analysis for mitigating noise impact in the maps, our first complementary investigation involved examining the impact of a stronger smoothing kernel. Specifically, we applied a Gaussian smoothing with a FWHM of 30 arcminutes to the realistic simulated data and evaluated the performance of CENN trained with it. As depicted in Figure 5, the results show a modest improvement in the recovered power spectra, with a mean absolute error of $0.5 \pm 0.1 \mu K^2$ for both E and B , and residuals of $10^{-1} \mu K^2$. However, this marginal gain came at the cost of losing information at the smallest angular scales, as expected from the increased smoothing. Despite this limitation, we note that employing a stronger smoothing could be a valuable strategy if the primary scientific goal is to establish upper limits on the CMB power spectra at certain multipoles, such as around the first acoustic peak, rather than a comprehensive recovery of the full angular power spectrum, particularly for the more challenging B modes.

³These methods are described in detail in [26].

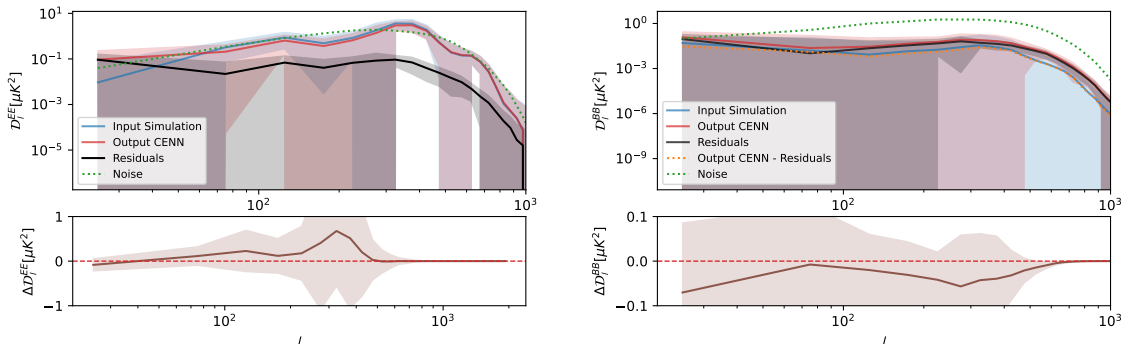


Figure 5. E and B mode power spectra recovering with CENN in a realistic case at $30'$ FWHM. Top left panel: comparison between the input E mode CMB spectra (in blue) and the output from the network (in red) The residuals are shown in black. Green dotted line represents the noise levels at 143 GHz. The bottom left panel represents the absolute difference between input and output spectra. Right panel describes the same analysis but for the B mode. The difference between output and residual spectra is plotted in the orange dotted line. Shaded areas show the 1σ standard deviation for each bin.

Secondly, we perform a kind of null-test, to verify the origin of the residual signals and the upper bound nature of CENN’s output. To this end, we applied the network to a validation dataset where the CMB signal was deliberately excluded, while retaining both foregrounds and noise. The resulting output power spectra, presented in Figure 6, is similar in shape but generally lower in amplitude compared to the residuals obtained in Section 4.2, especially for the E mode. This finding is significant for two key reasons: Firstly, it provides compelling evidence that a substantial portion of the residuals observed in the realistic case are indeed attributable to the instrumental noise, which CENN, to some extent, misinterprets as a genuine CMB signal. Secondly, and perhaps more importantly for observational cosmology, this null-test demonstrates that the CENN output will not produce a spurious CMB signal exceeding the level obtained when the true CMB is present in the input data. This characteristic is essential for the reliable derivation of upper limits on the CMB power spectra, particularly for the faint B modes, if applying CENN to real observational data, as it allows us to be confident that the recovered signal represents a conservative estimate of the true CMB.

5 Conclusions

In this work, we have presented a mathematical model based on neural networks, called the cosmic microwave background extraction neural network (CENN), which demonstrates promising capabilities for component separation in polarized microwave maps, extending the findings of a previous study focused on temperature. Our analysis, conducted using realistic simulations of the Planck sky including CMB, foregrounds (interstellar dust, synchrotron emission, and radio point sources), and instrumental noise at Planck levels, yielded several key insights.

Firstly, in an ideal scenario, devoid of instrumental noise, CENN demonstrates a promising ability to separate the polarized CMB signal from foreground emissions, even for the B modes, obtaining a mean absolute error (the difference between input and output spectra)

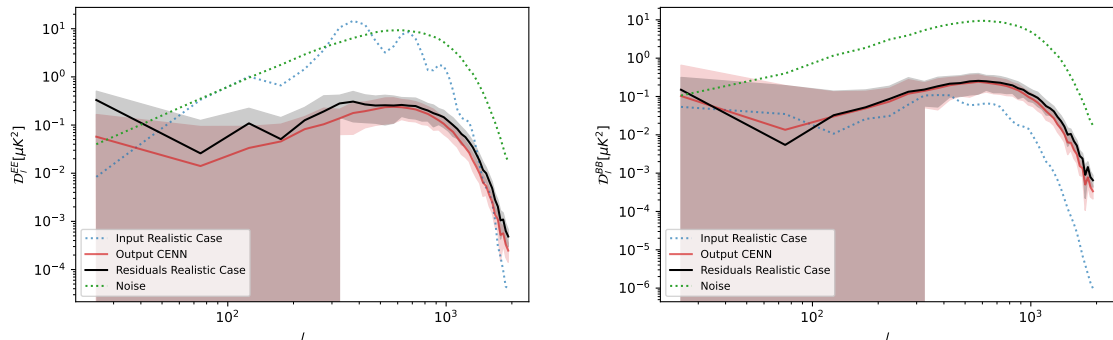


Figure 6. E and B mode power spectra recovering with CENN in a realistic kind of null-test (without input simulated CMB) case at 15' FWHM. Top left panel: comparison between the hypothetical input E mode CMB spectra (in dotted blue line) and the output from the network (in red). The residuals from the 15' case in Section 4.2 are shown in black. Green dotted line represents the noise levels at 143 GHz. The bottom left panel represents the absolute difference between hypothetical input and output spectra. Right panel describes the same analysis but for the B mode. Shaded areas show the 1σ standard deviation for each bin.

of about $0.1 \pm 0.3 \mu K^2$ for both modes, and residuals between 10^{-2} and $10^{-1} \mu K^2$ for E and around $10^{-2} \mu K^2$ for B . Moreover, our investigation into a realistic scenario incorporating Planck-level instrumental noise revealed that the increased residual power of about $10^{-1} \mu K^2$ for both modes, compared to an ideal noise-free case, is primarily attributable to the introduction of this noise. This observation has significant implications for future CMB experiments with higher sensitivity (i.e., lower noise levels) than Planck, suggesting that CENN's performance in recovering the CMB polarization could substantially improve, potentially approaching the lower residual levels observed in ideal simulations.

Secondly, we found that at large angular scales, the residual levels remained comparable to the ideal case with only residual foregrounds contamination below $l \sim 80$. This reinforces the conclusion that performance at the largest scales is more intrinsically linked to the finite patch size, suggesting that instrumental noise does not significantly impede CENN's ability to mitigate foregrounds at these scales.

Thirdly, our analysis of the residuals in the realistic case highlighted that while the B mode is more affected by both instrumental noise and foregrounds, the network output (indicated by the orange dotted line in Figure 4) demonstrates a tendency to preserve the underlying CMB signal, even when it is subdominant to the instrumental noise. This robustness implies that the recovered CMB signal in the output likely represents an upper bound on the true CMB signal in the presence of significant noise. Furthermore, our attempt to use a secondary neural network to further clean the CENN outputs from residuals yielded similar results to the initial CENN output. We interpret this as an indication that, with the current CENN architecture and the noise levels inherent in the Planck experiment, we are likely approaching the statistical limit for extracting the CMB signal, particularly for the faint B modes.

In terms of additional tests, we explored the impact of stronger smoothing (30' FWHM), which led to a minimal improvement in the recovered power spectra with a mean absolute error of $0.05 \pm 0.1 \mu K^2$ for both modes, and with similar residuals, at the cost of losing resolution at the smallest angular scales. However, this approach could be valuable for obtaining upper

limits at specific multipoles, such as around the first acoustic peak. Finally, a crucial kind of null-test, where CENN was applied to simulated maps without the CMB signal, revealed output power spectra similar but lower than the residuals in the realistic case. This confirms that a significant portion of the residuals are indeed due to instrumental noise mistakenly identified as CMB by the network. Importantly, this test also demonstrates that CENN will not produce a spurious CMB signal higher than that obtained when the true CMB is present, a vital characteristic for the reliable derivation of upper limits if applying this methodology to real data.

In conclusion, these results further support the potential of neural networks like CENN as promising component separation models for CMB polarization data, especially for future experiments with enhanced sensitivity. While current limitations, particularly concerning low signal-to-noise regimes and large angular scales with the present methodology, exist, the demonstrated ability to preserve the CMB signal and the insights gained regarding the impact of instrumental noise are valuable steps towards their application in next-generation CMB surveys.

Acknowledgments

JMC, LB and JGN acknowledge the CNS2022-135748 project funded by MCIN/AEI/10.13039/501100011033. JMC, LB, JGN, MMC and DC acknowledge the PID2021-125630NB-I00 project funded by MCIN/AEI/10.13039/501100011033/FEDER, UE. JMC and SRC also acknowledge the SV-PA-21-AYUD/2021/51301 grant. GP acknowledges support from Italian Research Center on High Performance Computing Big Data and Quantum Computing (ICSC), project funded by European Union NextGenerationEU and National Recovery and Resilience Plan (NRRP) Mission 4 Component 2 within the activities of Spoke 3 (Astrophysics and Cosmos Observations). CB acknowledges support from the COSMOS project of the Italian Space Agency, and the INDARK Initiative of the INFN. CGC and FJDC acknowledge the PID2021-127331NB-I00 project funded by MCIN/AEI/10.13039/501100011033/FEDER UE.

This research has made use of the packages `Matplotlib` [27], `Keras` [28], `Numpy` [29], `Namaster` [23], `HEALPix` [30] and `Healpy` [31] packages.

References

- [1] S. Weinberg, *Cosmology* (2008).
- [2] W. Hu and M. White, *A CMB polarization primer*, *NA* **2** (1997) 323 [[astro-ph/9706147](#)].
- [3] M. Zaldarriaga and U. Seljak, *All-sky analysis of polarization in the microwave background*, *Phys. Rev. D* **55** (1997) 1830 [[astro-ph/9609170](#)].
- [4] Planck Collaboration, N. Aghanim, Y. Akrami, F. Arroja, M. Ashdown, J. Aumont et al., *Planck 2018 results. I. Overview and the cosmological legacy of Planck*, *A&A* **641** (2020) A1 [[1807.06205](#)].
- [5] P. Ade, J. Aguirre, Z. Ahmed, S. Aiola, A. Ali, D. Alonso et al., *The simons observatory: science goals and forecasts*, *Journal of Cosmology and Astroparticle Physics* **2019** (2019) 056–056.
- [6] LiteBIRD Collaboration, E. Allys, K. Arnold, J. Aumont, R. Aurlen, S. Azzoni et al., *Probing Cosmic Inflation with the LiteBIRD Cosmic Microwave Background Polarization Survey*, *arXiv e-prints* (2022) [arXiv:2202.02773](#) [[2202.02773](#)].

- [7] N. Krachmalnicoff, C. Baccigalupi, J. Aumont, M. Bersanelli and A. Mennella, *Characterization of foreground emission on degree angular scales for CMB B-mode observations. Thermal dust and synchrotron signal from Planck and WMAP data*, *A&A* **588** (2016) A65 [[1511.00532](#)].
- [8] G. Puglisi, V. Galluzzi, L. Bonavera, J. Gonzalez-Nuevo, A. Lapi, M. Massardi et al., *Forecasting the Contribution of Polarized Extragalactic Radio Sources in CMB Observations*, *ApJ* **858** (2018) 85 [[1712.09639](#)].
- [9] U. Fuskeland, J. Aumont, R. Aurlien, C. Baccigalupi, A.J. Banday, H.K. Eriksen et al., *Tensor-to-scalar ratio forecasts for extended LiteBIRD frequency configurations*, *arXiv e-prints* (2023) [arXiv:2302.05228](#) [[2302.05228](#)].
- [10] M.J. Smith and J.E. Geach, *Astronomia ex machina: a history, primer and outlook on neural networks in astronomy*, *Royal Society Open Science* **10** (2023) 221454 [[2211.03796](#)].
- [11] I.J. Goodfellow, Y. Bengio and A. Courville, *Deep Learning*, MIT Press, Cambridge, MA, USA (2016).
- [12] M.A. Petroff, G.E. Addison, C.L. Bennett and J.L. Weiland, *Full-sky cosmic microwave background foreground cleaning using machine learning*, *The Astrophysical Journal* **903** (2020) 104.
- [13] G.-J. Wang, H.-L. Shi, Y.-P. Yan, J.-Q. Xia, Y.-Y. Zhao, S.-Y. Li et al., *Recovering the CMB Signal with Machine Learning*, *ApJS* **260** (2022) 13 [[2204.01820](#)].
- [14] Y.-P. Yan, G.-J. Wang, S.-Y. Li and J.-Q. Xia, *Recovering CMB Polarization Signals with Machine Learning*, *arXiv e-prints* (2023) [arXiv:2302.13572](#) [[2302.13572](#)].
- [15] J.M. Casas, L. Bonavera, J. González-Nuevo, C. Baccigalupi, M.M. Cueli, D. Crespo et al., *CENN: A fully convolutional neural network for CMB recovery in realistic microwave sky simulations*, *A&A* **666** (2022) A89 [[2205.05623](#)].
- [16] Planck Collaboration, Y. Akrami, M. Ashdown, J. Aumont, C. Baccigalupi, M. Ballardini et al., *Planck 2018 results. IV. Diffuse component separation*, *A&A* **641** (2020) A4 [[1807.06208](#)].
- [17] N. Krachmalnicoff and G. Puglisi, *ForSE: A GAN-based Algorithm for Extending CMB Foreground Models to Subdegree Angular Scales*, *ApJ* **911** (2021) 42 [[2011.02221](#)].
- [18] M. Tucci, L. Toffolatti, G. de Zotti and E. Martínez-González, *High-frequency predictions for number counts and spectral properties of extragalactic radio sources. New evidence of a break at mm wavelengths in spectra of bright blazar sources*, *A&A* **533** (2011) A57 [[1103.5707](#)].
- [19] J. González-Nuevo, L. Toffolatti and F. Argüeso, *Predictions of the Angular Power Spectrum of Clustered Extragalactic Point Sources at Cosmic Microwave Background Frequencies from Flat and All-Sky Two-dimensional Simulations*, *ApJ* **621** (2005) 1 [[astro-ph/0405553](#)].
- [20] J. Long, E. Shelhamer and T. Darrell, *Fully convolutional networks for semantic segmentation*, in *Proceedings of the IEEE conference on computer vision and pattern recognition*, pp. 3431–3440, 2015.
- [21] O. Ronneberger, P. Fischer and T. Brox, *U-Net: Convolutional networks for biomedical image segmentation*, *Medical Image Computing and Computer-Assisted Intervention – MICCAI 2015* (2015) .
- [22] I.J. Goodfellow, *Technical report: Multidimensional, downsampled convolution for autoencoders*, Tech. Rep. Université de Montréal (2010).
- [23] D. Alonso, J. Sanchez, A. Slosar and LSST Dark Energy Science Collaboration, *A unified pseudo- C_ℓ framework*, *MNRAS* **484** (2019) 4127 [[1809.09603](#)].
- [24] Planck Collaboration, R. Adam, P.A.R. Ade, N. Aghanim, M. Arnaud, M. Ashdown et al., *Planck 2015 results. IX. Diffuse component separation: CMB maps*, *A&A* **594** (2016) A9 [[1502.05956](#)].

- [25] Planck Collaboration, R. Adam, P.A.R. Ade, N. Aghanim, M.I.R. Alves, M. Arnaud et al., *Planck 2015 results. X. Diffuse component separation: Foreground maps*, *A&A* **594** (2016) A10 [[1502.01588](#)].
- [26] Planck Collaboration, R. Adam, P.A.R. Ade, N. Aghanim, M. Arnaud, M. Ashdown et al., *Planck 2015 results. IX. Diffuse component separation: CMB maps*, *A&A* **594** (2016) A9 [[1502.05956](#)].
- [27] J.D. Hunter, *Matplotlib: A 2d graphics environment*, *Computing In Science & Engineering* **9** (2007) 90.
- [28] F. Chollet, “Keras.” <https://github.com/fchollet/keras>, 2015.
- [29] T. Oliphant, “NumPy: A guide to NumPy.” USA: Trelgol Publishing, 2006.
- [30] K.M. Górski, E. Hivon, A.J. Banday, B.D. Wandelt, F.K. Hansen, M. Reinecke et al., *HEALPix: A Framework for High-Resolution Discretization and Fast Analysis of Data Distributed on the Sphere*, *ApJ* **622** (2005) 759 [[astro-ph/0409513](#)].
- [31] A. Zonca, L.P. Singer, D. Lenz, M. Reinecke, C. Rosset, E. Hivon et al., *healpy: equal area pixelization and spherical harmonics transforms for data on the sphere in python*, *Journal of Open Source Software* **4** (2019) 1298.